Materials Today: Proceedings 20 (2020) 605–610

Contents lists available at ScienceDirect

Materials Today: Proceedings

journal homepage: www.elsevier.com/locate/matpr

Fabrication and investigation of hybrid Perovskite solar cells based on porous silicon

Kawther A. Khalaph [a,*], Zainab J. Shanan [a], Falah Mustafa Al-Attar [b], Ahmed N Abd [c], Aqel Mashot Jafar [b]

[a] Department of Physics, College of Science for Women, University of Baghdad, Higher Education and Scientific Research Ministry, Iraq
[b] Solar Energy Research Center, Renewable Energy Directorate, Higher Education and Scientific Research Ministry, Baghdad, Iraq
[c] Department of Physics, College of Science, Al- Mustansiriyah University, Baghdad, Iraq

ARTICLE INFO

Article history:
Received 9 July 2019
Received in revised form 9 September 2019
Accepted 29 September 2019
Available online 1 November 2019

Keywords:
Porous silicon
Nanoparticle
Perovskite
FSEM
PCE

ABSTRACT

The present work is a study of the effect of incorporating (CuO/PbI2/CH3NH3I/ZnO) on the porous silicon (p-Psi) by using the drop casting technique procedure at a temperature of 70 °C. Structural, optical and morphological properties of (p-PSi, CuO, and ZnO) nanoparticles were characterized by X-ray diffraction, UV–Vis spectrophotometer, scanning electron microscopy and atomic force microscopy. The estimated optical energy value of thin films (CuO, PbI_2, and ZnO) was (3.87, 2.3, and 4.1 eV), respectively. The results of the current–voltage test manifested that the maximum power conversion efficiency (PCE) of the solar cell was 8.21%, and the filling factor was 41.4%. This research is revealing and investigating the successful hybrid Perovskite solar cells based on the porous silicon.

Selection and peer-review under responsibility of the scientific committee of the 2nd International Conference on Materials Engineering & Science.

1. Introduction

The material of high-efficiency solar cells absorbs light over a wide spectral range, generates high-efficiency shipments, and recharges these generated charges to electrodes with lower losses [1]. The ability to achieve straight pores makes the porous silicon a good material for the deposition of various metals [2], whereas the state of the fusion of nanostructures with the semiconductor substrate leads to a hybrid material, which provides the electronic properties of silicon and the nano behavior of sediments. Perovskite from semiconductors has attracted a great deal of attention due to its high absorption of light that makes it used in solar cells [3–5]. In recent years, the demand for nanostructured materials has increased significantly not only due to the development of the devices, but also because of the appearance of modified physical properties of nanoparticles compared to their bulk materials [2]. The properties of semiconductors materials (CuO, ZnO) are nontoxic and low cost; they have attracted a lot of attention because of their potential applications on solar cells, gas sensor, due to their photochemical properties and photoconductive [6,7]. This research is revealing and investigating the successful hybrid perovskite solar cells based on the porous silicon, as well as studying the properties of their materials.

2. Experimental procedure

2.1. Prepared of porous silicon (p-Psi)

An electrode instrument was used to manufacture porous silicon (p-PSi) using substrate silicon wafer (p-type) with an electrolytic Teflon cell containing 48% hydrofluoric acid and 99.9% purity ethanol with volume 1:2, as shown Fig. 1. The fabricated sample was processed from silicon monocrystalline with 10 μm resistivity and orientation of (1 0 0). The chemical process for p-Psi was to make a guard using current 10 mA/cm^2 for time 10 min and after that, a thin film layer of aluminium (about 200 nm) was deposited on the back surface using thermal evaporation technique [8,9].

2.2. Prepared of (CuO, ZnO) nanoparticles by chemical reaction

CuO NPs were manufactured using a chemical precipitation method. In a typical synthesis, 1.2 M of copper nitrate [Cu $(NO_3)_2$·$2H_2O$] was dissolved in (100 mL) of distilled water, which was agitated with magnetic stirring for 15 min until it completely dissolved. 1 M from sodium hydroxide (NaOH) solution was

* Corresponding author.
E-mail address: kawther75910@gmail.com (K.A. Khalaph).

https://doi.org/10.1016/j.matpr.2019.09.197
2214-7853/
Selection and peer-review under responsibility of the scientific committee of the 2nd International Conference on Materials Engineering & Science.

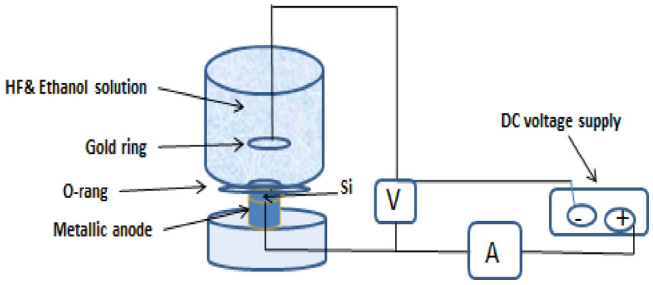

Fig. 1. The schematic diagram of the ECE system.

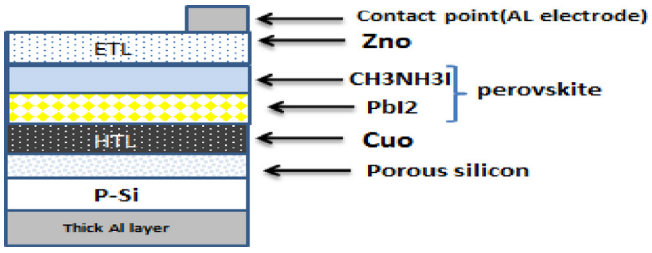

Fig. 2. Diagram of Photo-Voltaic showing (CuO/PbI2/CH3NH3I/ZnO) layer deposited on porous silicon.

dissolved in (100 mL) of distilled water, then the mixture was added by drop in [Cu $(NO_3)_2{\cdot}2H_2O$] solution under continuous stirring for 60 min and heated at 60 °C. The reaction mixture formed a solution with a bluish color and then was washed with distilled water several times to remove the native impurities in the product [3,10]. Also, it was then dried at 90–100 °C for 1 h. Finally, the precipitate was placed in a hot air oven at 200 °C for 2 h, at which the color changed to black.

ZnO NPs were synthesized by chemical precipitation method [11]. In a typical synthesis, 1 M of zinc sulphate heptahydrate $ZnSO_4{\cdot}7H_2O$ was dissolved in 100 mL of distilled water and 1 M sodium hydroxide (NaOH) solution was dissolved in 100 mL of distilled water which stirred with magnetic stirring for 15 min until they completely dissolved. The NaOH solution was dropped in $ZnSO_4{\cdot}7H_2O$ solution under continuous stirring for 60 min. The buffer was dropped wise in the solutions and stirred well until white, which indicated the gelatinous precipitates. The sediment was filtered, washed with distilled water and then dried at 90–100 °C for 1 h. Finally, the precipitate was placed in a hot air oven at 450 °C for 2 h.

2.3. The preparation of $MAPbI_3$-film

To prepared the PbI2 solution, we dissolved 0.153 g of the powder PbI2 in 10 mL of anhydrous N, N Dimethyl Formamide (DMF) (Sigma Aldrich). There are two typical approaches to the deposition of the Perovskite layer, one-step, and two-step coating. The first method, the Perovskite is formed by a spin-coating for mixed CH3NH3I and PbI2 solution (one-step coating). The second method, Perovskite is also prepared using a spin – coating but CH3NH3I is coated after PbI2 coating (two-step coating). A previous report showed that full coverage of Perovskite film on the surface of the substrate is necessary to ensure adequate shunt resistance and indicates that control of Perovskite film morphology is crucial in achieving high efficiency of Perovskite solar cells [1].

2.4. PV device fabrication

The precursor solution of (CuO, p-type) [10] was deposited by drop-casting on pre-heated transparent conductive p-type porous silicon (p-PSi) 50 °C, and then sintering substrates at 300 °C, time sintering time is 10 min. The hot substrates are left to cold at room temperature. Following by, the perovskite precursor solution is deposited by drop-casting on pre-heated ((p-PSi)/CuO) substrates at 100 °C. Following by depositing (ZnO, n-type) [12] precursor solution by drop-casting process and annealing at 100 °C, to obtain

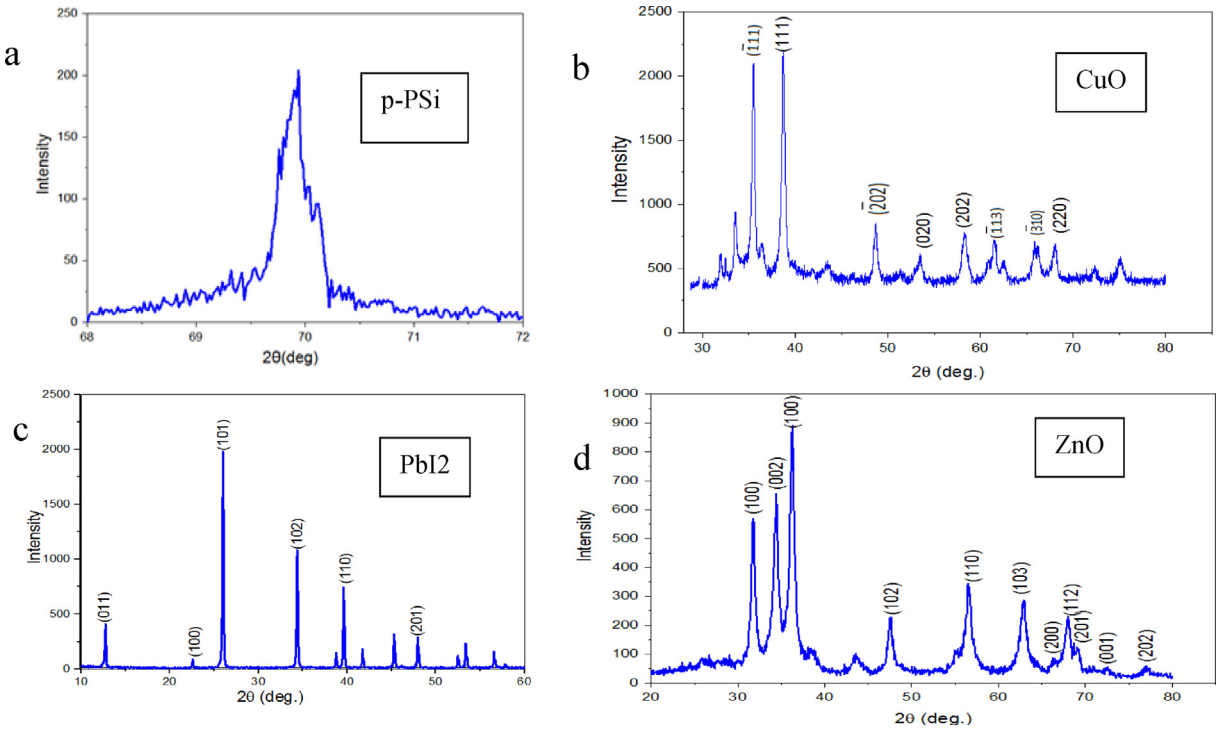

Fig. 3. The XRD patterns of (a) p-Psi, (b) CuO nanoparticle, (c) PbI_2 and (d) ZnO nanoparticle.

Table 1
2θ, FWHM, d-value and crystalline size.

sample	2θ (deg)	FWHM (deg)	d-value (A°)	size of crystalline (nm)
p-Si	69.34	0.23	1.35	42.05
	69.87	0.24	1.34	39.17
CuO	25.71	0.25	3.46	32.67
	35.47	0.31	2.52	26.20
	38.68	0.40	2.32	20.94
PbI2	21.35	0.15	4.15	52.97
	24.03	0.13	3.69	58.58
	28.92	0.15	3.08	53.40
ZnO	31.75	0.53	2.81	15.48
	34.38	0.65	2.60	12.81
	36.24	0.60	2.47	13.81

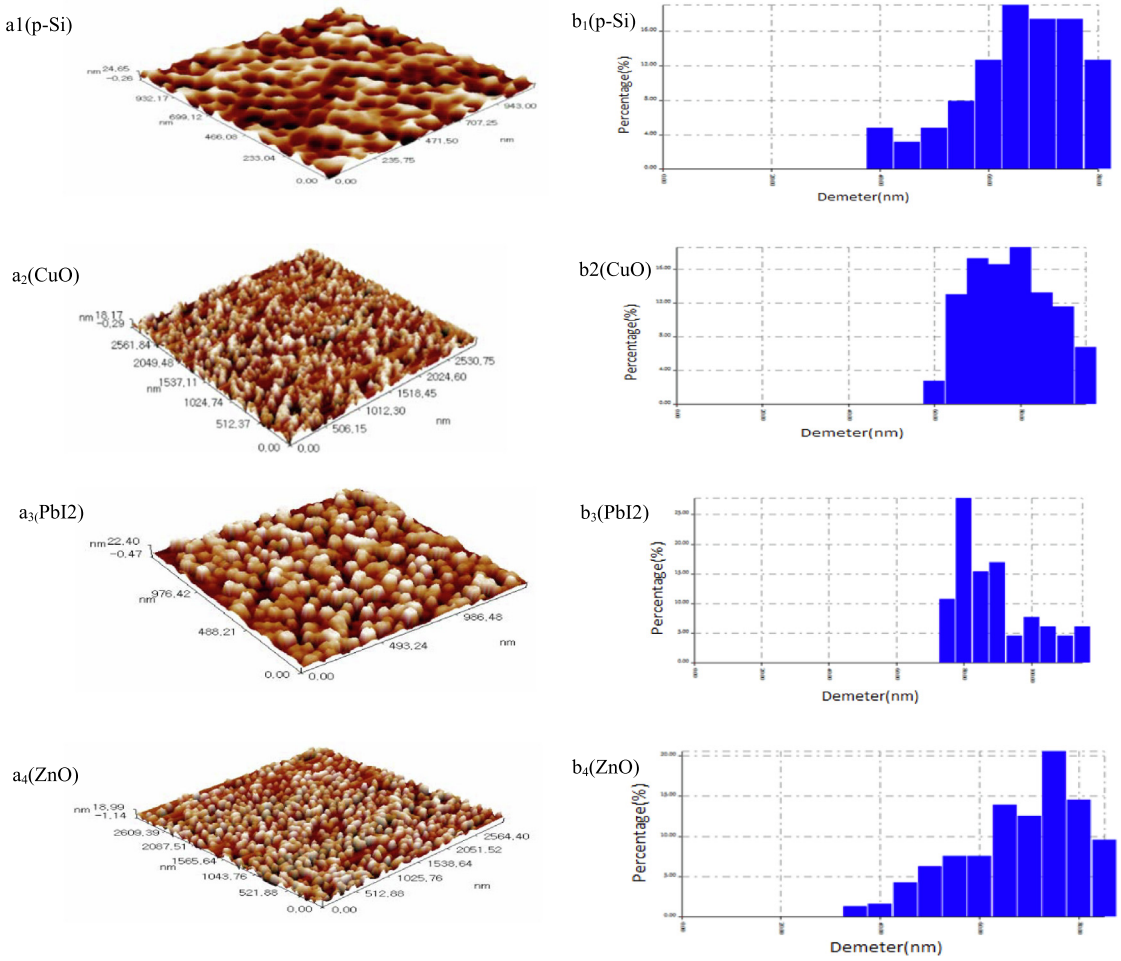

Fig. 4. Shows (a) 3D AFM image and (b) Distribution of granular accumulation chart of samples.

the samples of ((p-PSi)/CuO /$CH_3NH_3PbX_3$/ ZnO), and put foil Al with area 0.1 cm^2 as electrodes on ZnO layer, [13] as shown in Fig. 2.

3. Results and discussion

The structural physical properties of the samples (p-Si, CuO, PbI_2, ZnO) were studied by using the characterization of samples by XRD [13]. Surface morphology and surface roughness were determined by the atomic force microscopy (AFM). The optical properties measurements with optical bandgap were obtained by UV–VIS spectrophotometer.

3.1. X-ray measurement

The X-ray diffraction patterns for the crystalline nature of the synthesized (p-PSi, CuO, PbI_2, and ZnO) are illustrated in Fig. 3. From this figure, it can be noted that the XRD patterns are matching with the powders value of (CuO, PbI_2, and ZnO) by the comparison with JCPDS No. 89-2531, JCPDS No. 07-0235, and JCPDS No. 36-1451, respectively. The X-ray patterns results manifested that the broadening of the diffraction peaks indicates the presence of nanostructure by using Eq. (1), Debye-Scherrer formula [5].

$$D = \frac{0.9\lambda}{\beta cos\theta} \quad (1)$$

Table 2
Average diameter, root mean square, and roughness density of thin films.

Sample	Average. Diameter (nm)	Root Mean Square (RMS) (nm)	Roughness density (nm)
p-Si	63.15	6.68	5.75
CuO	75.34	5.16	4.45
PbI2	86.80	6.47	5.55
ZnO	65.30	5.94	5.19

where (D) is the crystalline size, (λ) is the wavelength (1.5406 °A) of X-ray, (θ) is the degree of the diffraction peak, and (β) is the full peak width at half maximum (FWHM).

The crystalline size of (p-PSi, CuO, PbI_2, and ZnO) shows that the sizes of prepared samples were within the nanoscale, as shown in Table 1.

3.2. AFM studies

Atomic force microscopy (AFM) is an instrument used to study the shape and texture of different surfaces. This method allows for diversity control and evaluation of the exact morphological properties of the sample, indicating better facilities than other microscopic methods. In AFM surface scanning in 3D, the image analysis allows to select; gives the mean root square roughness, the average particle height and intensity spectra of periodicity in the order of particles [9,13]. Using appropriate software, it is possible to evaluate the properties, such as roughness, porosity, medium size, and particle size distribution which affect the optical, electrical, mechanical, magnetic properties of the sample surface. Fig. 4 reveals the (3D) AFM images and the distribution of granular accumulation of films (p-Psi, CuO, PbI_2, and ZnO). The atomic force microscope images gave the information on the morphology of surface roughness, root mean square (RMS), and the roughness density of thin films, as listed in Table 2.

From the root mean square (RMS), known as the standard deviation of surface height from average height, the surface roughness can be measured. Surface roughness is determined by measuring the standard deviation of surface irregularities for several curves or curve averages. In general, the higher the roughness of the surface, the lower the RMS value, the lower light emission from the optical surface, resulting in improved surface quality [7]. This factor is used in the distribution of random surface irregularities.

3.3. FESEM of (CuO, PbI_2, ZnO, MAPbI3)

The FSEM images of nanostructured thin films as – prepared (CuO, PbI_2, and ZnO) with two different magnifications. The Fig. 5a–d showed that the shape of the nanoparticles (CuO, PbI_2) was rectangles, while ZnO [13] was sheets and the perovskite was almost spherical.

3.4. Optical properties

Fig. 6a shows the optical absorption of (CuO, PbI_2, and ZnO) films that were measured within a wavelength range (200–1100 nm) by using the UV–VIS double beam UVD-3500 (Labomed, Inc.).From the shoulder or peak spectra, the absorption edges of the samples can be used to estimate the gap by extrapolating the linear portion of the curve [8]. From the absorption peak, the energy band gap was calculated using Eq. (2) [14]:

$$(\alpha h\upsilon) = B * (h\upsilon - Eg)^n \quad (2)$$

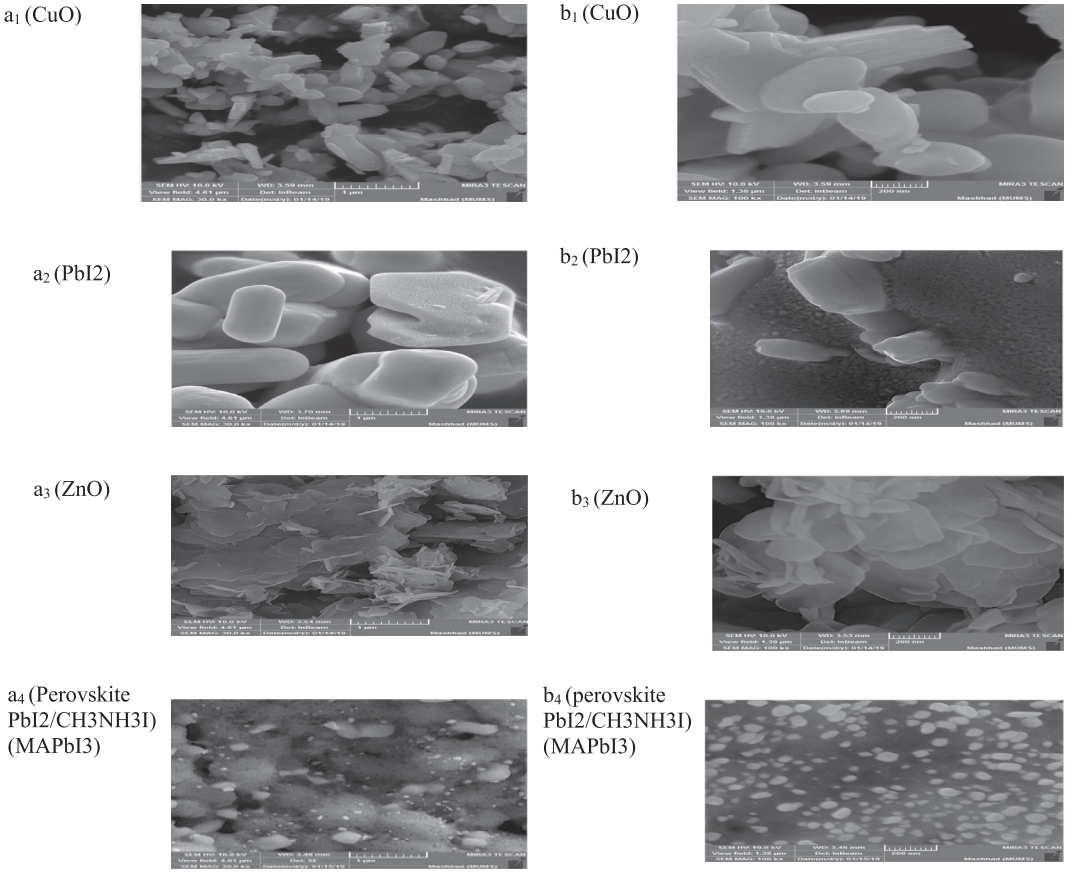

Fig. 5. High-resolution of (a) FESEM images measurement (1 μm) and (b) FESEM images measurement (200 nm).

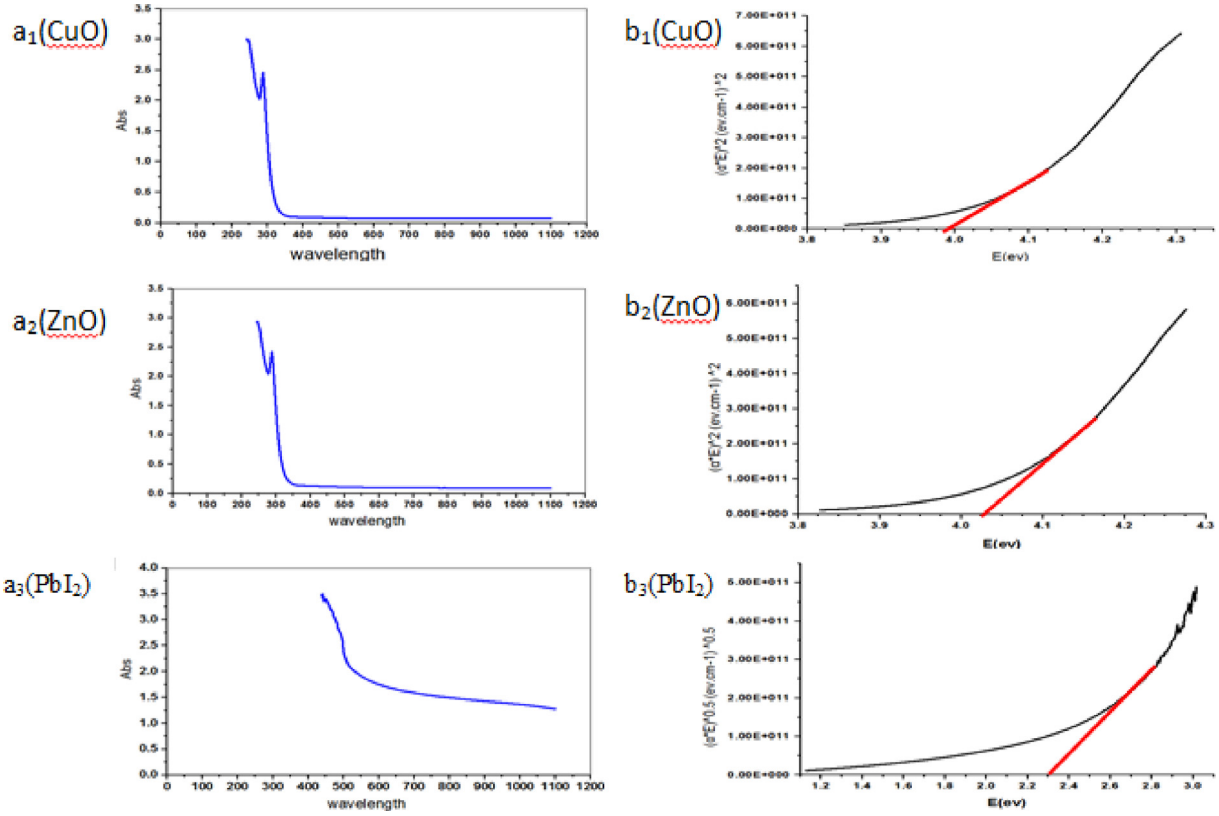

Fig. 6. (a) Optical absorption and (b) Energy gap of films.

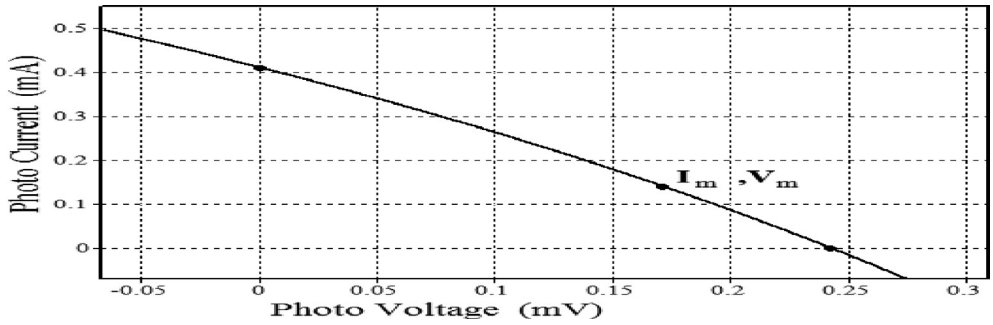

Fig. 7. I-V curve of perovskite solar cell.

where, (α) is the absorbance coefficient, (h) is the plank's constant, (B) is the empirical constant, (ν) is the light frequency, (n) is constant, which depends on the transmission either (1/2) for direct and (2) for indirect and Eg is the energy band gap.

It can be seen from Fig. 6b that the band gap of (CuO, ZnO) NPs was direct, whereas the band gap of (PbI_2) was indirect. The estimated value of band gap for (CuO, PbI_2, and ZnO) was (3.87, 2.3, and 4.1 eV), respectively, as shown in Fig. 6b. The thickness of sample was confirmed as an important parameter for estimating the Eg and was measured (t_{CuO} = 148.5 nm, t_{PbI2} = 400 nm, and t_{ZnO} = 149.5 nm). The lowest energy optical transition (electrons) from the valence band to the conduction band will increase, effectively increasing the band gap (Eg) [7]. Quantum confinement affects the increasing of band gap energies in nanostructures (CuO, ZnO) due to the reduced size of structures. These results correspond to the results of XRD, AFM, and FESEM.

3.5. Power conversion efficiency measurement (PCE)

Fig. 7 exhibits the PCE properties of the cell (CuO/PbI_2/CH_3NH_3I/ZnO) and the measured open-circuit voltage, short-circuit current, fill factor (F.F.), and efficiency.

All results suggest that the sandwich structure (CuO, PbI_2, CH_3NH_3I, and ZnO) can be used as highly efficient perovskite solar cells. The PCE and F.F. of a solar cell were calculated using Eqs. (3) and (4)[14]:

$$\mathbf{PCE} = \frac{\mathbf{V_{0c} \cdot I_{SC} \cdot FF / A_{SC}}}{\mathbf{P_{in}\ mw/cm^2}} \tag{3}$$

$$\text{F.F.} = \frac{I_m V_m}{I_{sc} V_{oc}} = \frac{P_m}{I_{sc} V_{oc}} \tag{4}$$

where, the open circuit voltage (V_{OC}), the short circuit current (I_{SC}) and the fill factor (F.F.) can be obtained at room temperature (300 K), and have the values (242 mV, 0.41 mA, and 41.4), respectively. The efficiency of the perovskite solar cell was 8.21%.

4. Conclusions

In this work, a perovskite solar cell was successfully manufactured. The results manifested that the characterizations of the prepared materials (CuO, ZnO) are nanostructures, which were used as electrodes of the solar cell. Copper oxide is a good holes extractor (HTL), while zinc oxide is used to extract the good electrons (ETL). From the results of power conversion efficiency (PCE), it is observed that the photovoltaic properties of the solar cell was improved using (CuO, ZnO) NPs and porous silicon.

References

[1] A. Belous, S. Kobylianska, O. V'yunov, P. Torchyniuk, V. Yukhymchuk, O. Hreshchuk, Effect of non-stoichiometry of initial reagents on morphological and structural properties of perovskites CH3NH3PbI3, Nanoscale Res. Lett. 14 (1) (2019) 4.
[2] P. Granitzer, K. Rumpf, T. Ohta, N. Koshida, P. Poelt, M. Reissner, "Porous silicon/Ni composites of high coercivity due to magnetic field-assisted etching",, Nanoscale Res. Lett. 7 (1) (2012) 384.
[3] L.-C. Chen, C.-Y. Weng, Optoelectronic properties of MAPbI3 perovskite/titanium dioxide heterostructures on porous silicon substrates for cyan sensor applications, Nanoscale Res. Lett. 10 (1) (2015) 404.
[4] J.-H. Im, J. Chung, S.-J. Kim, N. Park, Synthesis, structure, and photovoltaic property of a nanocrystalline 2H perovskite-type novel sensitizer (CH3CH2NH3)PbI3, Nanoscale Res. Lett. 7 (1) (2012) 353.
[5] T. Hamatani, Y. Shirahata, Y. Ohishi, M. Fukaya, T. Oku, Arsenic and chlorine co-doping to CH3NH3PbI3 perovskite solar cells, Adv. Mater. Phys. Chem. 07 (01) (2017) 1–10.
[6] H. Woo, B. Mohan, E. Heo, J.C. Park, H. Song, K.H. Park, CuO hollow nanosphere-catalyzed cross-coupling of aryl iodides with thiols, Nanoscale Res. Lett. (2013) 1–7.
[7] W. Wang et al., Nonuniform effect of carrier separation efficiency and light absorption in type-II perovskite nanowire solar cells, Nanoscale Res. Lett. 12 (1) (2017) 160.
[8] T. Defforge, M. Capelle, F. Tran-Van, G. Gautier, Plasma-deposited fluoropolymer film mask for local porous silicon formation, Nanoscale Res. Lett. 7 (2012) 1–8.
[9] C.-M. Chou, H.-T. Cho, V.K.S. Hsiao, K.-T. Yong, W.-C. Law, Quantum dot-doped porous silicon metal–semiconductor metal photodetector, Nanoscale Res. Lett. 7 (1) (2012) 291.
[10] L.C. Chen et al., Nano-structured CuO-Cu2O complex thin film for application in CH3NH3PbI3 perovskite solar cells, Nanoscale Res. Lett. 11 (1) (2016).
[11] D. Xrd, A.C. Mohan, B. Renjanadevi, Preparation of Zinc Oxide Nanoparticles and its Characterization Using Scanning Electron Microscopy (SEM) and X-Ray, Procedia Technol. 24 (2016) 761–766.
[12] S.K. Shrama, N. Saurakhiya, S. Barthwal, R. Kumar, A. Sharma, Tuning of structural, optical, and magnetic properties of ultrathin and thin ZnO nanowire arrays for nano device applications, Nanoscale Res. Lett. 9 (1) (2014) 1–17.
[13] A.A. Umar, M.Y.A. Rahman, R. Taslim, M.M. Salleh, M. Oyama, A simple route to vertical array of quasi-1d zno nanofilms on fto surfaces: 1d-crystal growth of nanoseeds under ammonia-assisted hydrolysis process, Nanoscale Res. Lett. 6 (2011) 1–12.
[14] M.H. Suhail, A.M. Jafar, Fabrication and characterization of organolead halide peroviske solar, Elixir Renew. Energy 98 (2016) 42709–42713.